NHC-CDI ligands boost multicarbon production on Cu electrocatalysts by increasing the accumulated surface charge and promoting *CO dimerization

Kirstine Nygaard Kolding,[1,2] Matias Bretlau,[2] Siqi Zhao,[3,4] Kristian Torbensen,[3,4] Kim Daasbjerg,[2,3,4] and Alonso Rosas-Hernández[1,2,4]*

[1]*Carbon Dioxide Activation Center (CADIAC), Interdisciplinary Nanoscience Center (iNANO), Aarhus University, 8000 Aarhus C, Denmark.*

[2]*Department of Chemistry, Aarhus University, 8000 Aarhus C, Denmark.*

[3]*Interdisciplinary Nanoscience Center (iNANO), Aarhus University, 8000 Aarhus C, Denmark.*

[4]*Novo Nordisk Foundation (NNF) CO_2 Research Center, Aarhus University, 8000 Aarhus C, Denmark.*

Email: arosas@chem.au.dk

Abstract

Copper-based materials have shown significant potential as catalysts for the electrochemical CO_2 reduction reaction (CO_2RR) due to their inherent ability to produce multicarbon products. The functionalization of Cu electrodes with organic additives represents a simple yet powerful strategy for improving the intrinsic activity of these electrocatalysts by tailoring the microenvironment around the Cu active sites to favor specific reaction pathways. In this work, we introduce NHC-CDI-functionalized Cu catalysts, which demonstrate a remarkable increase in activity for multicarbon product formation, surpassing bare Cu electrodes by more than an order of magnitude. These hybrid catalysts operate efficiently in a gas diffusion configuration, achieving a multicarbon product selectivity of 58% with a partial current density of −80

mA/cm^2. Using modified pulsed voltammetry measurements, we found that the activity for multicarbon product formation is closely linked to the surface charge that accumulates during electrocatalysis, resulting from the buildup of CO_2RR intermediates. We further supported our findings with in situ Raman spectroscopy measurements, which unveiled a preference for carbon monoxide binding on Cu step sites, which are known to promote C–C coupling, in the best-performing hybrid catalysts. Additionally, we observed a general preference for atop-bound *CO intermediates over bridge-bound ones in the molecularly functionalized catalysts. Our study underscores the significant potential of molecular tuning in developing efficient electrocatalysts for CO_2 reduction and emphasizes the utility of surface charge as a descriptor of multicarbon product activity.

Introduction

The ongoing climate crisis has underscored our need to accelerate the transition towards carbon-neutral pathways to produce fuels and chemical feedstocks.[1–3] We require efficient technologies that promote the decentralized conversion of renewable energies into stable and easily transportable energy carriers, thus facilitating the sustainable growth of society. The electrochemical CO_2 reduction reaction (CO_2RR) represents a promising approach for seasonal energy storage, allowing for the conversion of wasteful CO_2 to value-added products as well as enabling closed-loop recycling of harmful CO_2 emissions. Cu-based catalysts hold a unique position in the field of CO_2RR due to their ability to produce multicarbon (C_{2+}) products at appreciable reaction rates.[4,5] The practical application of Cu-based catalysts faces limitations, requiring intensive research into developing highly selective and stable Cu-based catalysts to efficiently produce hydrocarbon products.[6] Such efforts are crucial for addressing the challenges posed by the climate crisis and advancing sustainable energy solutions.

Over the years, several strategies to improve the electrochemical performance of Cu catalysts have been devised, a frequent one being the nanostructuring of the catalyst surface.[7] While the introduction of unique architectures on the nanoscale has been shown to increase the overall performance of the catalyst, this strategy leaves the intrinsic activity of the catalyst unchanged, and the enhanced performance is merely due to an increase in surface area.[6] In order to alter the intrinsic activity of the catalysts, strategies are required to change the binding environment for CO_2RR intermediates, thereby breaking the thermodynamic scaling relations that govern the adsorption energy of reduction intermediates.[8,9] Such approaches include doping of Cu substrates with other elements to introduce distinct binding sites,[10–12] the utilization of tandem systems in which the reduction of CO_2 to CO and the further reduction of CO into multicarbon products are decoupled and hence facilitated at lower overpotential,[13–16] and the introduction of molecular surface additives to alter the microenvironment at the catalytic active sites.

The molecular modification of metal surfaces represents a promising strategy and has, in several examples, been shown to increase the intrinsic activity of electrocatalysts via secondary coordination sphere interactions with key reaction intermediates, hydrophobicity effects, or surface charge rearrangements.[17–21] For instance, Wang and coworkers demonstrated that introducing amino acids on Cu surfaces leads to a significantly enhanced hydrocarbon production and attributed this to stabilizing hydrogen bond interactions between the *CHO reduction intermediate and the $-NH_3^+$ moieties of the amino acids.[20] Peters and coworkers used arylpyridinium additives to stabilize atop-bound CO intermediates, thereby increasing ethylene production.[17,22] In more recent work, Lim and coworkers found that histidine-functionalization of Cu_2O catalysts increased the surface charge accumulated during catalysis compared to non-modified Cu_2O and used this as a descriptor for the enhanced catalytic activity observed with the functionalized electrodes.[21]

In this work, we exploited *N*-heterocyclic carbene-carbodiimide (NHC-CDI) ligands as molecular additives on Cu catalysts and obtained remarkable improvements of over tenfold in the intrinsic current density of C_{2+} products in an H-cell setup. The best-performing hybrid catalyst demonstrated a Faradaic efficiency (FE) of 58% for C_{2+} products at a total current density of −132 mA/cm^2 at −1.06 V in a GDE-based setup. This provides proof of concept for the application of these hybrid catalysts in high-performing CO_2 flow electrolyzers. Using a modified pulsed voltammetry method (mPV), we uncovered a correlation between the surface charge accumulated during electrocatalysis and the observed activity for all tested catalysts. Improvements in hybrid electrodes are often attributed to hydrophobicity effects that shift the CO_2/H_2O ratio at the electrode surface. Furthermore, in situ Raman spectroscopy revealed that the hybrid Cu catalysts exhibit a preference for surface-adsorbed carbon monoxide (*CO) in an atop configuration over a bridge-bound one. Notably, the best-performing hybrid catalysts showed a higher proportion of *CO on Cu step sites, underlining the role of NHC-CDI ligands in selectively stabilizing CO on Cu active sites with higher reactivity towards C-C coupling reactions.

Results and Discussion

Synthesis of NHC-CDI ligands

We synthesized all NHC-CDI ligands following the general procedure shown in Scheme 1. This synthetic pathway entailed coupling the relevant *N,N*-disubstituted imidazolium salt with the diarylcarbodiimide precursor.[23,24] The syntheses of these starting materials are described in the Supplementary Information (Section S3). Initial deprotonation of the C2 carbon in the *N,N*-disubstituted imidazolium salt by potassium *tert*-butoxide leads to the generation of the corresponding *N*-heterocyclic carbene. The carbene reacts in situ upon adding the electrophilic carbodiimide reagent to form the NHC-CDI ligand. The generated carbenes are highly susceptible

to degradation upon exposure to ambient conditions, and maintaining an inert environment during the reaction is critical. Low yields were observed if the carbenes had been exposed to room temperature for extended periods, and the less bulky *N,N*-dimethyl-substituted carbene was found to be particularly temperature sensitive, leading to low yields if the solution reached room temperature. The main degradation pathway for the carbenes is expected to be the coupling of two carbenes to form the inactive dimer (the Wanzlick equilibrium),[25,26] explaining why the more sterically hindered carbenes were more robust in terms of temperature sensitivity. Good yields (77-98%) were observed for all NHC-CDI ligands except **NHC-CDI 4**, which was afforded a 20% yield. This was mainly due to a more extensive purification procedure requiring several recrystallizations. All NHC-CDI ligands have been characterized by ^{1}H NMR, ^{13}C NMR, ATR-FTIR, and HR-MS (found in the Supplementary Information).

Scheme 1. General synthesis pathway for the preparation of NHC-CDI ligands. The yields are given after each ligand entry.

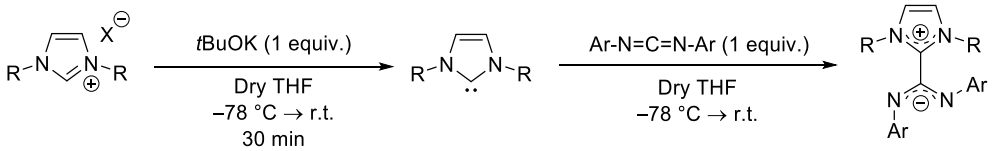

1: R = methyl, Ar = 2,6-diisopropylphenyl, 79%
2: R = cyclohexyl, Ar = 2,6-diisopropylphenyl, 77%
3: R = methyl, Ar = 2,6-dimethylphenyl, 98%
4: R = 2,6-diisopropylphenyl, Ar = 2,6-dimethylphenyl, 20%
5: R = 2,6-diisopropylphenyl, Ar = phenyl, 90%

Preparation of hybrid NHC-CDI-Cu catalysts and optimization of electrodeposition conditions

The NHC-CDI ligands were used as molecular additives on Cu electrodes via an electrodeposition method. Using $CuSO_4 \cdot 5H_2O$ as the copper source, Cu particles were electrodeposited onto Cu foil under acidic conditions and at constant current (–2 mA/cm^2) in the presence of an NHC-CDI ligand, leading to the incorporation of the ligand on the catalyst surface. For bare Cu samples, the electrodeposition took place in the absence of the ligand using otherwise the

same conditions. The electrodeposition conditions were optimized with respect to ligand concentration ([NHC-CDI]), total electrodeposition charge (C_{ed}), and ligand-to-$CuSO_4{\cdot}5H_2O$ ratio (NHC-CDI/Cu) to achieve the highest activity for multicarbon (C_{2+}) products. The electrochemical testing of the hybrid catalysts in CO_2RR was performed using a CO_2-fed H-cell at constant potential. Ligand **2** was used in all optimization experiments, and the conditions identified for this ligand were then used to test the remaining NHC-CDI ligands. Figure 1a shows the effect of changing the concentration of **2** while keeping a constant concentration of $CuSO_4{\cdot}5H_2O$ (90 mM) on the partial current densities of each product ($j_{product}$). Focusing on the partial current density for ethylene, j_{C2H4}, we obtain a volcano plot with the highest value at a ligand concentration of 5 mM in the electrodeposition solution. A similar trend is observed for the activity for all combined C_{2+} products, where j_{C2+} increases from –0.15 mA/cm^2 for the bare Cu sample to –0.65 mA/cm^2 at a 5 mM concentration, corresponding to more than a 4-fold enhancement. A plot of FEs yields the same results with a ligand concentration in the electrodeposition bath of 5 mM corresponding to the highest FE for C_{2+} products (Supplementary Figure S1). Optimization plots for C_{ed} and NHC-CDI/Cu can be found in the Supplementary Information (Figure S2-4). The optimum conditions were identified as 2 C/cm^2 and 1:18 for C_{ed} and NHC-CDI/Cu, respectively, in terms of both j_{C2+} and FE(C_{2+}). This corresponds to [$CuSO_4{\cdot}5H_2O$] = 90 mM and [**2**] = 5 mM.

Under these optimal conditions for the electrodeposition of ligand **2**, we next investigated the effect of the electrolysis potential on the CO_2RR performance. Unless otherwise stated, all potentials are reported versus the reversible hydrogen electrode (RHE). As seen in Figure 1b, three different potentials were tested, obtaining the highest value of j_{C2+} (–0.65 mA/cm^2) at –1.06 V. Multicarbon product formation was significantly reduced at –0.99 V (j_{C2+} = –0.14 mA/cm^2) while it was similar at –1.13 V (j_{C2+} = –0.59 mA/cm^2), although with a substantial increase in H_2 production. Thus, further electrocatalytic evaluations were carried out at –1.06

V. In summary, the optimum electrodeposition and electrolysis conditions were identified as [$CuSO_4 \cdot 5H_2O$] = 90 mM, [NHC-CDI] = 5 mM, C_{ed} = 2 C/cm^2, and E = –1.06 V. These conditions were employed in the preparation and electrochemical testing of the remaining NHC-CDI ligands. The hybrid catalysts are referred to **Cu-1-5**, depending on the ligand used in the preparation.

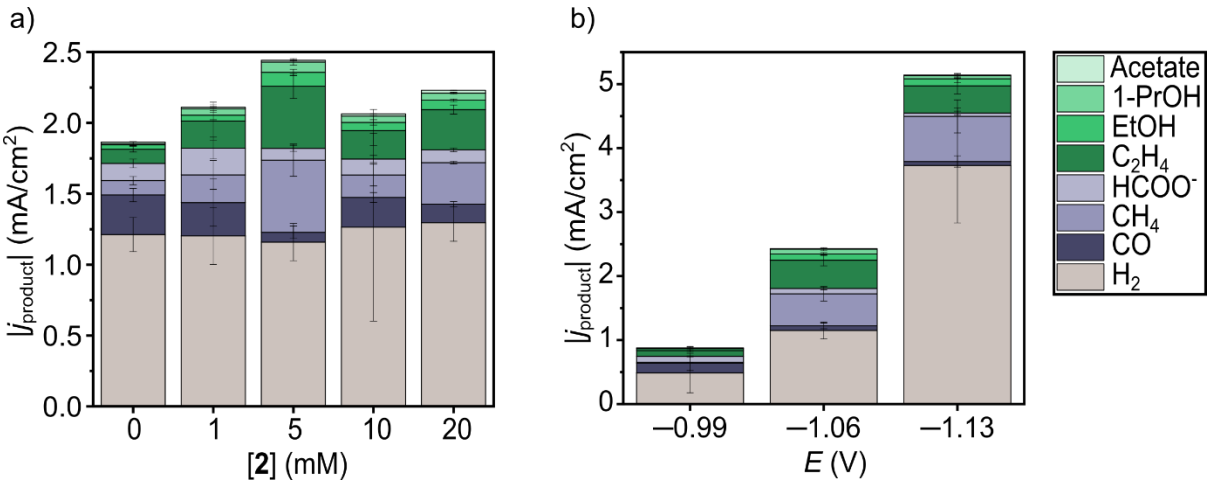

Figure 1. a) Electrocatalytic performance of hybrid catalyst **Cu-2** in CO_2RR at –1.06 V using different concentrations of **2** during the electrodeposition step. b) Effect of the electrolysis potential on the partial current densities of different CO_2RR products with a ligand concentration of 5 mM. In both bases, [$CuSO_4 \cdot 5H_2O$] = 90 mM and C_{ed} = 2 C/cm^2.

Electrochemical performance of Cu-NHC-CDI catalysts in the CO_2RR

The performance of the hybrid catalysts in CO_2RR was determined by constant potential electrolysis experiments at –1.06 V. Importantly, to establish that the intrinsic activity of the functionalized electrodes was improved in comparison to bare Cu (**Cu**), we normalized the current density with respect to the electrochemically active surface area (ECSA). The ECSA of the hybrid electrodes was estimated via the capacitance method, in which the double-layer capacitance of the system is measured and related to the ECSA (see Supplementary Information for details).[27] The normalized current densities with the ECSA (j_{ECSA}) for C_{2+} and C_1 products are shown in Figure 2a-b. A higher value of $j_{ECSA,C2+}$ is obtained for all Cu-NHC-CDI samples

compared to **Cu**, indicating that the hybrid catalysts possess a higher intrinsic activity for producing multicarbon products. The best-performing sample is **Cu-3**, which generates a partial current density of –0.61 mA/cm^2 for C_{2+} products, corresponding to a 10-fold increase compared to **Cu** ($j_{ECSA,C2+}$ = –0.056 mA/cm^2). **Cu-1**, **Cu-2**, **Cu-4**, and **Cu-5** produce 8-, 4-, 3-, and 2-fold increases in $j_{ECSA,C2+}$, respectively, and the performance of the tested catalysts hence follows the order **Cu-3** > **Cu-1** > **Cu-2** ~ **Cu-4** > **Cu-5** > **Cu**. The major C_{2+} product is ethylene. Interestingly, a concomitant decrease in the production of CO is observed for all hybrid catalysts relative to **Cu**. In contrast, the production of all other C_1 products increases (Figure 2b). This suggests that, as expected, the improved electrocatalytic activity towards C_{2+} products is a consequence of the enhanced dimerization of *CO, which is a step in the C_{2+} product pathway. The dimerization of *CO or its coupling with hydrogenated derivatives (*CHO, *COH) is believed to constitute the rate-determining step in the pathway towards C_{2+} products.[28,29] Conversely, the activity towards H_2 increases with the hybrid samples, ruling out that the observed catalytic changes are due to suppression of the hydrogen evolution reaction (HER) (Supplementary Figure S5-6). Only **Cu-5** exhibits similar activity for the HER, and this catalyst also displays the lowest activity for C_{2+} products of all hybrid catalysts, thus supporting the independence of these two processes.

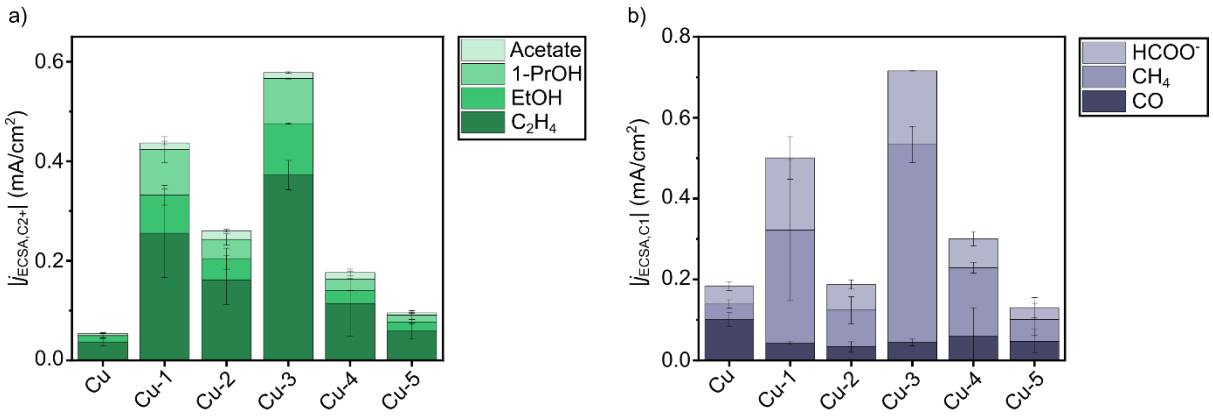

Figure 2. Electrochemical performance of **Cu-1-5** and bare **Cu** sample. Partial current density for a) C_{2+} products and b) C_1 products. In both plots, currents are normalized with respect to the ECSA.

To confirm that the CO_2RR products observed are genuinely derived from the reduction of CO_2 and not due to the NHC-CDI ligands' degradation, control experiments were performed using **Cu-3** as the model sample (Supplementary Section S4.3). These experiments assessed the electrochemical performance in an argon-purged phosphate buffer electrolyte (pH = 6.8), resulting in the exclusive generation of H_2. These results show that incorporating NHC-CDI ligands into Cu-based catalysts boosts C_{2+} reaction rates and enhances the overall catalyst activity.

To demonstrate the ability of NHC-CDI molecular additives to enhance C_{2+} product formation in higher-performing configurations, ligand **3** was used to prepare hybrid Cu-based gas diffusion electrodes (GDEs) to be tested in a flow cell electrolyzer. **Cu$_{GDE}$-3** and a bare reference, **Cu$_{GDE}$**, were prepared using Cu/PTFE substrates in a similar way as the Cu foil catalysts with slight modifications to the electrodeposition procedure to accommodate the Cu/PTFE substrate (see the Supplementary Information for details). The CO_2RR performance of the catalysts was evaluated in a CO_2 flow cell electrolyzer at –1.06 V with 1.0 M $KHCO_3$ as electrolyte. In line with the H-cell experiments, **Cu$_{GDE}$-3** substantially improved its performance relative to **Cu$_{GDE}$**, increasing FE(C_{2+}) from 33% to 58% (Figure 3a). With **Cu$_{GDE}$-3**, ethylene becomes the predominant reduction product with a FE(C_2H_4) of 42%. **Cu$_{GDE}$-3** generates a total current density of –132 mA/cm^2 and j_{C2+} = –77 mA/cm^2, which is more than twice that produced by **Cu$_{GDE}$** (j_{C2+} = –33 mA/cm^2) (Figure 3b). Additionally, the production of H_2 in terms of both the FE and current density is approximately the same for the two catalysts, indicating that the enhanced CO_2RR performance is not due to HER suppression, which is in accordance with the H-cell experiments. The results presented in this section provide proof of concept for the application of Cu-NHC-CDI catalysts as high-performing electrodes in CO_2 flow electrolyzers.

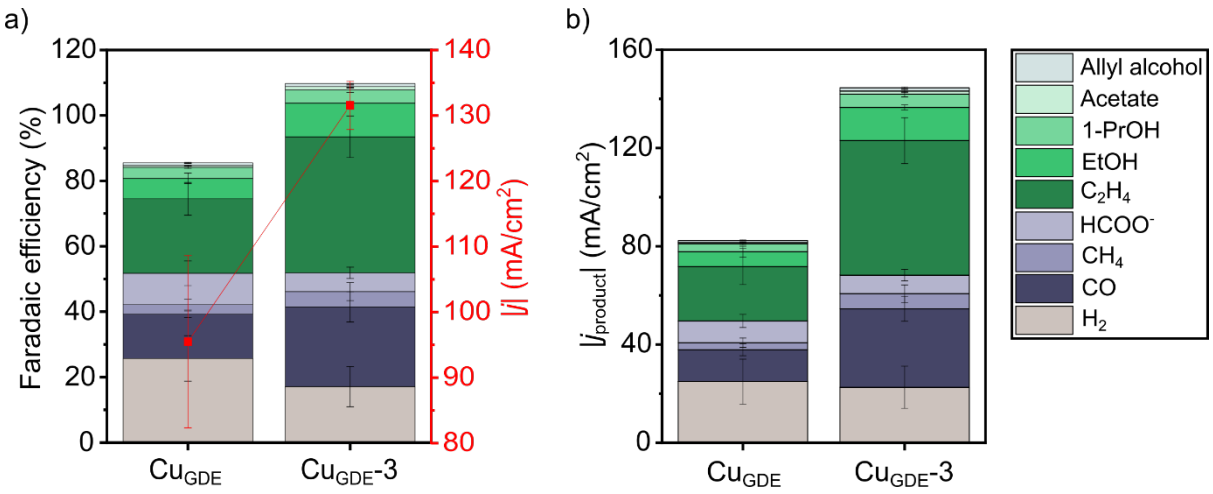

Figure 3. Electrochemical performance of **Cu$_{GDE}$** and **Cu$_{GDE}$-3** in a GDE-based setup using a liquid-electrolyte gas diffusion CO_2 electrolyzer. The plots show a) the FE of all reduction products (left axis) and the total current density (right axis), and b) the partial current density of reduction products for each sample. In both cases, current densities are normalized with respect to the geometric area of the electrode (A = 0.785 cm^2).

Surface characterization of hybrid catalysts and further insights

Catalyst surfaces were characterized by scanning electron microscopy (SEM) to investigate morphological features that may explain the difference in catalytic properties of chosen samples. Figure 4a-c shows SEM images of **Cu**, **Cu-3**, and **Cu-5**, representing the control, best-performing, and worst-performing hybrid samples. All three samples exhibited microstructuring on the surface, yet the features on **Cu** appear more well-defined than on the hybrid samples. The hybrid samples display similar morphologies distinct from the features observed on **Cu**. While these differences may contribute to the enhanced catalytic properties of the hybrid samples compared to **Cu**, it does not explain the marked increase in activity observed for **Cu-3** relative to **Cu-5**. SEM images at lower magnification reveal overall uniform surfaces with similar macroscopic features between all samples (Supplementary Table S7). Hence, other experimental methods are required to explain the catalytic behavior of the hybrid catalysts.

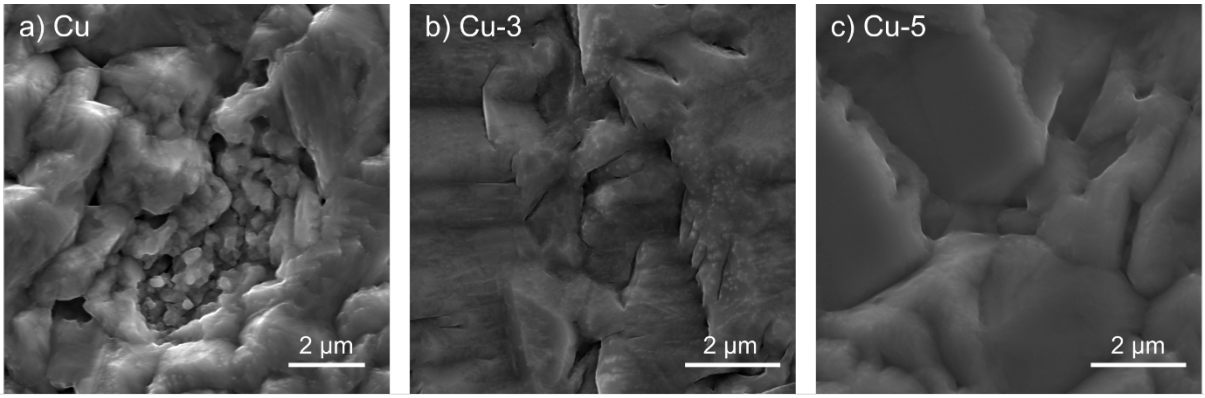

Figure 4. SEM images of a) **Cu**, b) **Cu-3**, and c) **Cu-5** representing the reference sample, the best-performing, and the worst-performing hybrid catalysts.

To confirm the presence of the NHC-CDI ligands on the surface of the catalysts, we used X-ray photoelectron spectroscopy (XPS). Accordingly, an N 1*s* peak for **Cu-3** and **Cu-5** samples was observed, whereas no signal was detected for the bare **Cu** (Supplementary Figure S17). A red line showing the average intensity of the N 1*s* signal is included in the plots to highlight the low-intensity peak for the hybrid catalysts. In the spectrum of **Cu**, the red line corresponds to the noise level throughout the plot, clearly showing the absence of a signal. The average intensity rather than the assumed baseline is depicted in the plots. This indicates the presence of the ligand on the hybrid catalyst surface. The low intensity of the signal is in line with the expectedly low surface concentration of the ligand. The presence of the ligands on the Cu surface was also corroborated by Raman spectroscopy measurements conducted on **Cu-3** and **Cu-5**. The Raman spectra of **Cu-3** and **Cu-5** show two signals at ~1435 cm^{-1} and ~1655 cm^{-1}, assigned to the C–C(N) stretch and the C=C ring stretch, respectively (Supplementary Figure S25).[30]

The Cu 2*p* spectra in Figure 5a show two narrow $2p_{3/2}$ and $2p_{1/2}$ peaks at 932.8 eV and 952.6 eV, respectively, for the three samples. Both signals indicate the presence of Cu^0 or Cu_2O since these two species have almost identical binding energies.[31] The narrow peak shape (full width at half max of ~0.83) of the Cu $2p_{3/2}$ peak and the lack of satellite peaks at higher binding

energies indicate that CuO is not present in significant amounts. The Cu LMM spectra provide a deeper insight into the oxidation state of the surface Cu species (Figure 5b). For the bare **Cu** and **Cu-5**, two roughly equal-sized signals were detected at 918.4 eV and 916.4 eV stemming from Cu^0 and Cu_2O, respectively. For **Cu-3**, Cu^0 is the dominating component, although smaller amounts of Cu_2O are also observed. Hence, the surface valence states differ between **Cu-3**, **Cu-5**, and **Cu**. These findings can explain the superior electrocatalytic activity of **Cu-3** compared to **Cu-5**. The lower content of Cu^+ surface states in **Cu-3** indicates that NHC-CDI ligand **3** effectively increases the electron density of the hybrid electrocatalyst through a charge transfer mechanism. The more electron-rich surface would be expected to stabilize *CO intermediates to a higher degree due to the increased π backbonding interaction between the CO 2π* orbital and the d-band from Cu.[32] This interaction strengthens the metal–carbon bond and weakens the C≡O bond, activating the intermediate toward dimerization. In the case of **Cu-5** and **Cu**, this stabilization is less prominent due to a lower surface concentration of the ligand or an intrinsically lower electron-donating ability, leading to lower activity for C_{2+} products.

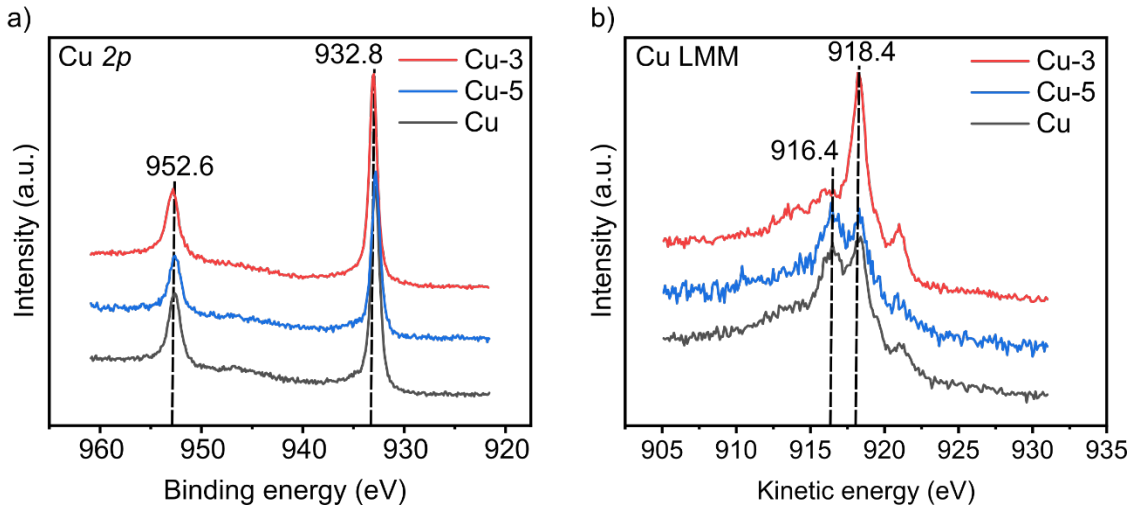

Figure 5. XPS spectra showing the a) Cu 2*p* and b) Cu LMM signals from **Cu**, **Cu-3**, and **Cu-5**. The intensity of individual spectra has been scaled to show the shift in binding/kinetic energy between samples.

Determination of surface charge by modified pulsed voltammetry

XPS measurements revealed a higher concentration of Cu^0 states in **Cu-3**, which can improve the stabilization of *CO and increase its coverage. To confirm this, we employed a modified pulsed voltammetry (mPV) technique to quantify the accumulation of charged species at the hybrid catalysts' surface during CO_2RR (see Supplementary Section S2.4 and S4.6 for details). Hence, estimating the electrocatalytic surface charge can offer valuable insights into the role of the surface ligands in the selective generation of multicarbon products. Figure 6a shows an example of the decay of the anodic current at a potential difference (ΔE) of 1.6 V, where the integrated area is shaded blue. The integrated anodic current corresponds to a charge (Q_{an}), which was normalized with respect to the ECSA of each catalyst ($Q_{an,ECSA}$) and plotted as a function of ΔE (Figure 6b). For all hybrid catalysts and bare **Cu**, volcano plots were obtained where the highest value of $Q_{an,ECSA}$ was observed close to ΔE = 1.6 V, corresponding to the surface charge accumulated at an operating potential of −1.06 V during bulk electrolysis. Notably, this potential value was identified as optimal during the electrocatalytic optimization using **Cu-2** to generate C_{2+} products (Figure 1b).

Plotting the $j_{C2+,ECSA}$ as a function of $Q_{an,ECSA}$ at ΔE = 1.6 V for all catalysts revealed a linear trend that provides crucial insight into the role of the NHC-CDI ligands in controlling the performance of the hybrid electrocatalysts (Figure 6c). Higher values of $Q_{an,ECSA}$ led to greater efficiencies for generating multicarbon products. This indicates that the best-performing samples, such as **Cu-1** and **Cu-3,** facilitate a higher population of charged intermediates at their surface than low-performing catalysts, such as **Cu** and **Cu-5**. This increased coverage of surface intermediates aligns with an enhanced *CO stabilization resulting from an electron-rich surface, as revealed by the XPS measurements.

To confirm that the observed trends in $Q_{an,ECSA}$ are due to CO_2RR intermediates, a control experiment was conducted with **Cu-3** in argon-purged phosphate buffer electrolyte at pH = 6.8 (Figure 6d). In this case, the volcano-plot behavior disappears, and the $Q_{an,ECSA}$ values were significantly lower at all potentials. The accumulated charge in this control experiment is likely due to background processes unrelated to the CO_2RR, such as HER and capacitive current. Overall, these results underscore the active role of NHC-CDI ligands in altering the surface of the hybrid electrocatalysts to increase the stabilization of CO_2RR intermediates, which is directly correlated with an increased generation of multicarbon products.

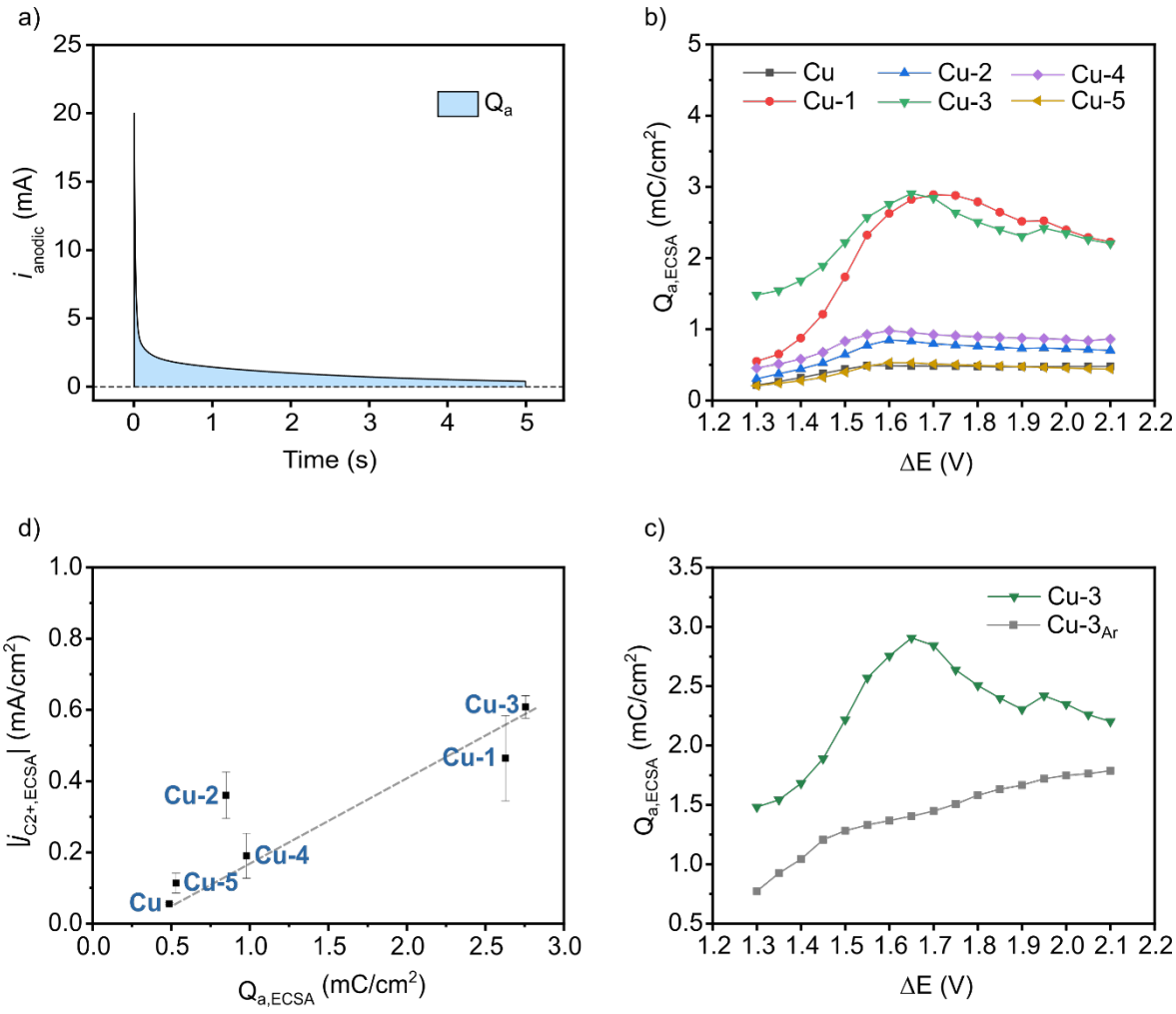

Figure 6. mPV results showing a) an example of the integrated area used to determine Q_a for **Cu-3** at ΔE = 1.6 V, b) $Q_{an,ECSA}$ as a function of ΔE for all catalysts, c) $j_{C2+,ECSA}$ as a function of $Q_{an,ECSA}$ for all hybrid catalysts, and d) control experiment conducted with **Cu-3** in Ar-purged phosphate buffer electrolyte (pH 6.8).

In Situ Raman Spectroscopy

The *CO intermediate is assumed to play a key role in the formation of C–C bonds during the CO_2RR,[28,29] hence studying this surface intermediate by in situ technologies can give access to valuable mechanistic insights. We next performed in situ Raman spectroscopy measurements to identify the surface intermediates present during the CO_2RR and, specifically, probe the behavior of *CO under catalytic conditions. Figure 7a-c shows the in situ Raman spectra of **Cu**, **Cu-3**, and **Cu-5** in the range 1760-2300 cm^{-1} at potentials ranging from –0.4 V to –1.3 V. In the spectra recorded using bare **Cu** (Figure 7a), a signal appears with Raman shift ~1900 cm^{-1} at a potential of –0.7 V and reaches its maximum at –1.1 V, attributed to the $*CO_{bridge}$ intermediate.[33–35] In previous reports, it was proposed that $*CO_{bridge}$ is inactive towards further reduction during CO_2RR due to a high energy barrier of the hydrogenation step to form the *CHO intermediate, which is important for C–C coupling.[28,33] Furthermore, the presence of $*CO_{bridge}$ alone as the only *CO intermediate has been suggested to suppress hydrocarbon formation, which explains the low activity towards C_{2+} products that we observed with the bare **Cu** sample.[35] For **Cu-3** and **Cu-5**, a broad band appears with a Raman shift >2000 cm^{-1} corresponding to the $*CO_{atop}$ intermediate (Figure 7b-c).[34,36] In contrast to the reactivity of $*CO_{bridge}$, $*CO_{atop}$ is an on-pathway intermediate believed to participate in the C–C coupling step either through a direct dimerization or via its hydrogenation to form *CHO/*COH intermediates.[28,33] The observation of this intermediate hence explains the difference in catalytic behavior between the bare and the hybrid Cu catalysts; the latter facilitates the formation of the active $*CO_{atop}$ over the largely inactive $*CO_{bridge}$, thereby enabling the dimerization to form C_{2+} products.

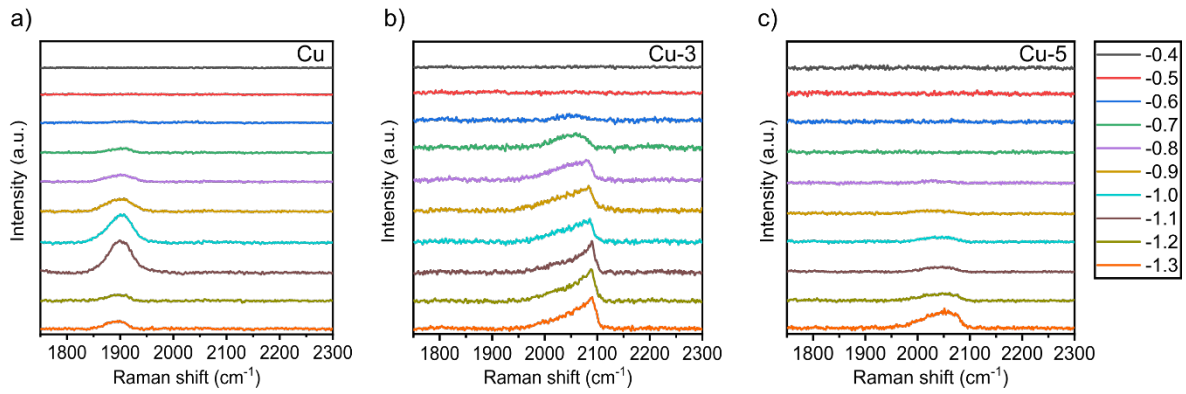

Figure 7. In situ Raman spectra obtained with a) **Cu**, b) **Cu-3**, and c) **Cu-5** at potentials ranging from –0.4 V to –1.3 V vs RHE.

The *CO_{atop} signals observed for **Cu-3** are blue-shifted compared to those seen for **Cu-5**, indicating *CO_{atop} species with different vibrating frequencies exist. The *CO_{atop} signal for **Cu-3** can be deconvoluted into a high-frequency band (HFB) and a low-frequency band (LFB) with Raman shifts at ~2085 cm^{-1} and ~2045 cm^{-1}, respectively (Figure 8a). These bands have been previously assigned to *CO coordinated on Cu terrace sites (LFB) or step sites (HFB), and thus depend on the facets present at the Cu surface.[37] Importantly, *CO at step sites (such as that between (100) and (111) planes) has been linked to greater production of C_{2+} products due to enhanced *CO dimerization.[38,39] Figure 8b shows the results from the deconvolution of the *CO_{atop} signal with the ratio between the area of the HFB and the total area of the signal as a function of the applied potential. The relative area of the HFB increases with more negative potentials and peaks at –1.2 V. This peak potential agrees with that identified in the mPV measurements, suggesting the central role of *CO as a source of the accumulating species during CO_2RR. The deconvolution of the *CO_{atop} signal from **Cu-5** gives only rise to a single low-frequency band located at ~2045 cm^{-1}, and, therefore, does not indicate the presence of any *CO species at step sites (Figure 8a). Collectively, these results suggest that the enhanced activity towards C_{2+} products observed for **Cu-3** is due to the superior *CO dimerization reactivity taking place on Cu step sites which are absent in the case of **Cu-5**, which only exhibits *CO

at terrace sites. Bare **Cu**, on the other hand, presents a poor activity for C_{2+} products due to the accumulation of the inactive $*CO_{bridge}$. Thus, our in situ Raman results do not only explain the enhanced activity observed between bare **Cu** and the hybrid samples, but they also provide evidence that accounts for the difference in activity between the hybrid samples due to the different coordination mode of *CO induced by the presence of NHC-CDI ligand **3**.

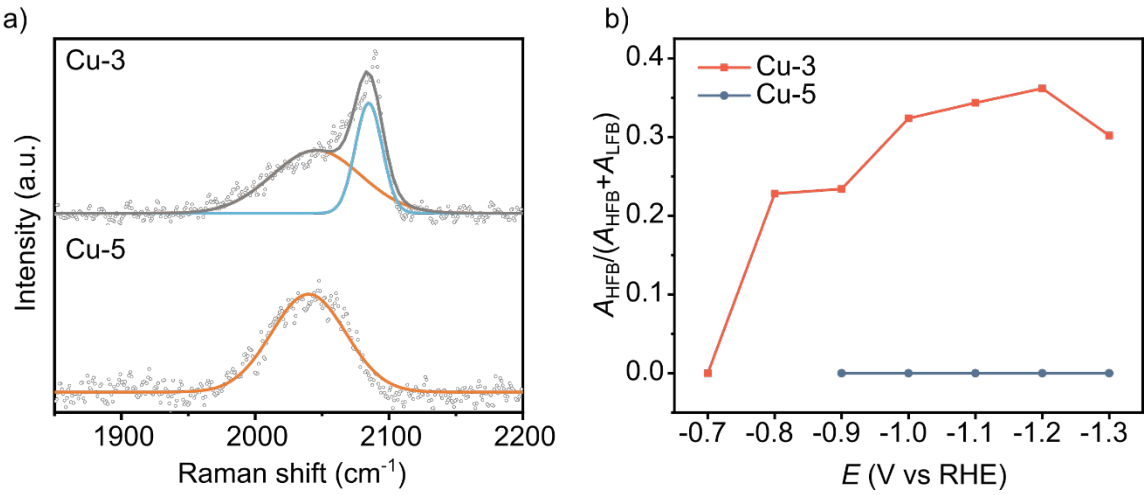

Figure 8. The deconvolution of Raman signals obtained with **Cu-3** and **Cu-5**. a) Example showing the deconvolution of the signals obtained at –1.1 V, and b) the area of the HFB relative to the total area of the signal as a function of applied potential.

Conclusion

In summary, this study introduces the use of NHC-CDI ligands as additives for Cu-based CO_2RR electrocatalysts. Following the electrodeposition of NHC-CDI ligands onto the Cu surface, the resulting hybrid Cu catalysts significantly enhance the activity for producing C_{2+} products, achieving more than a tenfold increase when compared to bare Cu in an H-cell setup. In tests conducted with a GDE-based electrolyzer, **Cu-3** demonstrated a FE(C_{2+}) of 58% and a total current density of −132 mA/cm^2 at −1.06 V, providing a proof of concept for the practical application of Cu-NHC-CDI catalysts as high-performing electrodes in CO_2 flow electrolyzers. We employed modified pulsed voltammetry measurements to assess the accumulation of

surface charge during catalysis, shedding light on the active role of NHC-CDI ligands in enhancing selectivity for multicarbon products. We established a correlation between the accumulated surface charge and the observed activity for C_{2+} products across all catalysts. Higher surface charge accumulation, attributed to electronic effects resulting from ligand modification, translates into improved reactivity for C_{2+} products. Deeper mechanistic insights were gained through in situ Raman spectroscopy, allowing us to propose that the increased C_{2+} product activity in **Cu-3** is due to enhanced *CO dimerization on Cu step sites, which are absent in the less effective hybrid **Cu-5** and bare Cu. The poorer performance of bare Cu is further explained by the presence of the inactive $*CO_{bridge}$ as the sole *CO intermediate. This work underscores the use of molecular additives to control the selectivity of Cu electrocatalysts by modifying their surface valence states and facilitating the stabilization of the critical *CO intermediate on highly active Cu sites for the production of multicarbon products.

Author contributions

A.R.-H. conceived and supervised the project. K.N.K. carried out ligand synthesis, catalyst preparation, electrochemical experiments, XPS measurements, and SEM/SEM-EDX experiments. M.B. carried out molecule synthesis. S.Z. conducted in situ Raman measurements. K.T. assisted in the catalytic evaluation of GDE samples. K.N.K. and A.R.-H. analyzed the data and wrote the manuscript. All authors contributed to the discussion and manuscript preparation.

Acknowledgements

We are deeply grateful for financial support from the Danish National Research Foundation (Grant No. DNRF118). The Carlsberg Foundation is acknowledged for funding the Tescan Clara SEM used in this work.

References

(1) Galán-Martín, Á.; Tulus, V.; Díaz, I.; Pozo, C.; Pérez-Ramírez, J.; Guillén-Gosálbez, G. Sustainability Footprints of a Renewable Carbon Transition for the Petrochemical Sector within Planetary Boundaries. *One Earth* **2021**, *4*, 565–583.

(2) Chu, S.; Cui, Y.; Liu, N. The Path towards Sustainable Energy. *Nat. Mater.* **2017**, *16*, 16–22.

(3) Schiffer, Z. J.; Manthiram, K. Electrification and Decarbonization of the Chemical Industry. *Joule* **2017**, *1*, 10–14.

(4) Hori, Y.; Kikuchi, K.; Murata, A.; Suzuki, S. Production of Methane and Ethylene in Electrochemical Reduction of Carbon Dioxide at Copper Electrode in Aqueous Hydrogencarbonate Solution. *Chem. Lett.* **1986**, *15*, 897–898.

(5) Kuhl, K. P.; Cave, E. R.; Abram, D. N.; Jaramillo, T. F. New Insights into the Electrochemical Reduction of Carbon Dioxide on Metallic Copper Surfaces. *Energy Environ. Sci.* **2012**, *5*, 7050.

(6) Nitopi, S.; Bertheussen, E.; Scott, S. B.; Liu, X.; Engstfeld, A. K.; Horch, S.; Seger, B.; Stephens, I. E. L.; Chan, K.; Hahn, C.; Nørskov, J. K.; Jaramillo, T. F.; Chorkendorff, I. Progress and Perspectives of Electrochemical CO_2 Reduction on Copper in Aqueous Electrolyte. *Chem. Rev.* **2019**, *119*, 7610–7672.

(7) Mistry, H.; Varela, A. S.; Kühl, S.; Strasser, P.; Cuenya, B. R. Nanostructured Electrocatalysts with Tunable Activity and Selectivity. *Nat. Rev. Mater.* **2016**, *1*, 1–14.

(8) Li, Y.; Sun, Q. Recent Advances in Breaking Scaling Relations for Effective Electrochemical Conversion of CO_2. *Adv. Energy Mater.* **2016**, *6*, 1600463.

(9) Abild-Pedersen, F.; Greeley, J.; Studt, F.; Rossmeisl, J.; Munter, T. R.; Moses, P. G.; Skúlason, E.; Bligaard, T.; Nørskov, J. K. Scaling Properties of Adsorption Energies for Hydrogen-Containing Molecules on Transition-Metal Surfaces. *Phys. Rev. Lett.* **2007**, *99*, 016105.

(10) Zhou, Y.; Che, F.; Liu, M.; Zou, C.; Liang, Z.; De Luna, P.; Yuan, H.; Li, J.; Wang, Z.; Xie, H.; Li, H.; Chen, P.; Bladt, E.; Quintero-Bermudez, R.; Sham, T.-K.; Bals, S.; Hofkens, J.; Sinton, D.; Chen, G.; Sargent, E. H. Dopant-Induced Electron Localization Drives CO_2 Reduction to C_2 Hydrocarbons. *Nat. Chem.* **2018**, *10*, 974–980.

(11) Wei, Z.; Ding, J.; Duan, X.; Chen, G.-L.; Wu, F.-Y.; Zhang, L.; Yang, X.; Zhang, Q.; He, Q.; Chen, Z.; Huang, J.; Hung, S.-F.; Yang, X.; Zhai, Y. Enhancing Selective Electrochemical CO_2 Reduction by In Situ Constructing Tensile-Strained Cu Catalysts. *ACS Catal.* **2023**, *13*, 4711–4718.

(12) Peng, C.; Luo, G.; Zhang, J.; Chen, M.; Wang, Z.; Sham, T.-K.; Zhang, L.; Li, Y.; Zheng, G. Double Sulfur Vacancies by Lithium Tuning Enhance CO_2 Electroreduction to N-Propanol. *Nat. Commun.* **2021**, *12*, 1580.

(13) Morales-Guio, C. G.; Cave, E. R.; Nitopi, S. A.; Feaster, J. T.; Wang, L.; Kuhl, K. P.; Jackson, A.; Johnson, N. C.; Abram, D. N.; Hatsukade, T.; Hahn, C.; Jaramillo, T. F.

Improved CO_2 Reduction Activity towards C_{2+} Alcohols on a Tandem Gold on Copper Electrocatalyst. *Nat. Catal.* **2018**, *1*, 764–771.

(14) Hoang, T. T. H.; Verma, S.; Ma, S.; Fister, T. T.; Timoshenko, J.; Frenkel, A. I.; Kenis, P. J. A.; Gewirth, A. A. Nanoporous Copper–Silver Alloys by Additive-Controlled Electrodeposition for the Selective Electroreduction of CO_2 to Ethylene and Ethanol. *J. Am. Chem. Soc.* **2018**, *140*, 5791–5797.

(15) Wang, M.; Nikolaou, V.; Loiudice, A.; Sharp, I. D.; Llobet, A.; Buonsanti, R. Tandem Electrocatalytic CO_2 Reduction with Fe-Porphyrins and Cu Nanocubes Enhances Ethylene Production. *Chem. Sci.* **2022**, *13*, 12673–12680.

(16) Li, F.; Li, Y. C.; Wang, Z.; Li, J.; Nam, D.-H.; Lum, Y.; Luo, M.; Wang, X.; Ozden, A.; Hung, S.-F.; Chen, B.; Wang, Y.; Wicks, J.; Xu, Y.; Li, Y.; Gabardo, C. M.; Dinh, C.-T.; Wang, Y.; Zhuang, T.-T.; Sinton, D.; Sargent, E. H. Cooperative CO_2-to-Ethanol Conversion via Enriched Intermediates at Molecule–Metal Catalyst Interfaces. *Nat. Catal.* **2020**, *3*, 75–82.

(17) Li, F.; Thevenon, A.; Rosas-Hernández, A.; Wang, Z.; Li, Y.; Gabardo, C. M.; Ozden, A.; Dinh, C. T.; Li, J.; Wang, Y.; Edwards, J. P.; Xu, Y.; McCallum, C.; Tao, L.; Liang, Z.-Q.; Luo, M.; Wang, X.; Li, H.; O'Brien, C. P.; Tan, C.-S.; Nam, D.-H.; Quintero-Bermudez, R.; Zhuang, T.-T.; Li, Y. C.; Han, Z.; Britt, R. D.; Sinton, D.; Agapie, T.; Peters, J. C.; Sargent, E. H. Molecular Tuning of CO_2-to-Ethylene Conversion. *Nature* **2020**, *577*, 509–513.

(18) Zhao, S.; Christensen, O.; Sun, Z.; Liang, H.; Bagger, A.; Torbensen, K.; Nazari, P.; Lauritsen, J. V.; Pedersen, S. U.; Rossmeisl, J.; Daasbjerg, K. Steering Carbon Dioxide Reduction toward C–C Coupling Using Copper Electrodes Modified with Porous Molecular Films. *Nat. Commun.* **2023**, *14*, 844.

(19) Liang, H.-Q.; Zhao, S.; Hu, X.-M.; Ceccato, M.; Skrydstrup, T.; Daasbjerg, K. Hydrophobic Copper Interfaces Boost Electroreduction of Carbon Dioxide to Ethylene in Water. *ACS Catal.* **2021**, *11*, 958–966.

(20) Xie, M. S.; Xia, B. Y.; Li, Y.; Yan, Y.; Yang, Y.; Sun, Q.; Chan, S. H.; Fisher, A.; Wang, X. Amino Acid Modified Copper Electrodes for the Enhanced Selective Electroreduction of Carbon Dioxide towards Hydrocarbons. *Energy Environ. Sci.* **2016**, *9*, 1687–1695.

(21) Lim, C. Y. J.; Yilmaz, M.; Arce-Ramos, J. M.; Handoko, A. D.; Teh, W. J.; Zheng, Y.; Khoo, Z. H. J.; Lin, M.; Isaacs, M.; Tam, T. L. D.; Bai, Y.; Ng, C. K.; Yeo, B. S.; Sankar, G.; Parkin, I. P.; Hippalgaonkar, K.; Sullivan, M. B.; Zhang, J.; Lim, Y.-F. Surface Charge as Activity Descriptors for Electrochemical CO_2 Reduction to Multi-Carbon Products on Organic-Functionalised Cu. *Nat. Commun.* **2023**, *14*, 335.

(22) Han, Z.; Kortlever, R.; Chen, H.-Y.; Peters, J. C.; Agapie, T. CO_2 Reduction Selective for $C_{\geq 2}$ Products on Polycrystalline Copper with N-Substituted Pyridinium Additives. *ACS Cent. Sci.* **2017**, *3*, 853–859.

(23) Martínez-Prieto, L. M.; Urbaneja, C.; Palma, P.; Cámpora, J.; Philippot, K.; Chaudret, B. A Betaine Adduct of N-Heterocyclic Carbene and Carbodiimide, an Efficient Ligand to Produce Ultra-Small Ruthenium Nanoparticles. *Chem. Commun.* **2015**, *51*, 4647–4650.

(24) Márquez, A.; Ávila, E.; Urbaneja, C.; Álvarez, E.; Palma, P.; Cámpora, J. Copper(I) Complexes of Zwitterionic Imidazolium-2-Amidinates, a Promising Class of Electroneutral, Amidinate-Type Ligands. *Inorg. Chem.* **2015**, *54*, 11007–11017.

(25) Wanzlick, H.-W.; Schikora, E. Ein nucleophiles Carben. *Chem. Ber.* **1961**, *94*, 2389–2393.

(26) Poater, A.; Ragone, F.; Giudice, S.; Costabile, C.; Dorta, R.; Nolan, S. P.; Cavallo, L. Thermodynamics of N-Heterocyclic Carbene Dimerization: The Balance of Sterics and Electronics. *Organometallics* **2008**, *27*, 2679–2681.

(27) McCrory, C. C. L.; Jung, S.; Ferrer, I. M.; Chatman, S. M.; Peters, J. C.; Jaramillo, T. F. Benchmarking Hydrogen Evolving Reaction and Oxygen Evolving Reaction Electrocatalysts for Solar Water Splitting Devices. *J. Am. Chem. Soc.* **2015**, *137*, 4347–4357.

(28) Todorova, T. K.; Schreiber, M. W.; Fontecave, M. Mechanistic Understanding of CO_2 Reduction Reaction (CO_2RR) Toward Multicarbon Products by Heterogeneous Copper-Based Catalysts. *ACS Catal.* **2020**, *10*, 1754–1768.

(29) Garza, A. J.; Bell, A. T.; Head-Gordon, M. Mechanism of CO_2 Reduction at Copper Surfaces: Pathways to C $_2$ Products. *ACS Catal.* **2018**, *8*, 1490–1499.

(30) Gucciardi, P. G.; Trusso, S.; Vasi, C.; Patanè, S.; Allegrini, M. Nano-Raman Imaging of Cu–TCNQ Clusters in TCNQ Thin Films by Scanning near-Field Optical Microscopy. *Phys. Chem. Chem. Phys.* **2002**, *4*, 2747–2753.

(31) Biesinger, M. C. Advanced Analysis of Copper X-Ray Photoelectron Spectra. *Surf. Interface Anal.* **2017**, *49*, 1325–1334.

(32) Hammer, B.; Morikawa, Y.; Nørskov, J. K. CO Chemisorption at Metal Surfaces and Overlayers. *Phys. Rev. Lett.* **1996**, *76*, 2141–2144.

(33) Gunathunge, C. M.; Ovalle, V. J.; Li, Y.; Janik, M. J.; Waegele, M. M. Existence of an Electrochemically Inert CO Population on Cu Electrodes in Alkaline pH. *ACS Catal.* **2018**, *8*, 7507–7516.

(34) An, H.; Wu, L.; Mandemaker, L. D. B.; Yang, S.; de Ruiter, J.; Wijten, J. H. J.; Janssens, J. C. L.; Hartman, T.; van der Stam, W.; Weckhuysen, B. M. Sub-Second Time-Resolved Surface-Enhanced Raman Spectroscopy Reveals Dynamic CO Intermediates during Electrochemical CO_2 Reduction on Copper. *Angew. Chem. Int. Ed.* **2021**, *60*, 16576–16584.

(35) Chou, T.-C.; Chang, C.-C.; Yu, H.-L.; Yu, W.-Y.; Dong, C.-L.; Velasco-Vélez, J.-J.; Chuang, C.-H.; Chen, L.-C.; Lee, J.-F.; Chen, J.-M.; Wu, H.-L. Controlling the Oxidation State of the Cu Electrode and Reaction Intermediates for Electrochemical CO_2 Reduction to Ethylene. *J. Am. Chem. Soc.* **2020**, *142*, 2857–2867.

(36) Chang, X.; Zhao, Y.; Xu, B. pH Dependence of Cu Surface Speciation in the Electrochemical CO Reduction Reaction. *ACS Catal.* **2020**, *10*, 13737–13747.

(37) Gunathunge, C. M.; Li, J.; Li, X.; Hong, J. J.; Waegele, M. M. Revealing the Predominant Surface Facets of Rough Cu Electrodes under Electrochemical Conditions. *ACS Catal.* **2020**, *10*, 6908–6923.

(38) Wu, Z.-Z.; Zhang, X.-L.; Niu, Z.-Z.; Gao, F.-Y.; Yang, P.-P.; Chi, L.-P.; Shi, L.; Wei, W.-S.; Liu, R.; Chen, Z.; Hu, S.; Zheng, X.; Gao, M.-R. Identification of Cu(100)/Cu(111) Interfaces as Superior Active Sites for CO Dimerization During CO_2 Electroreduction. *J. Am. Chem. Soc.* **2022**, *144*, 259–269.

(39) Malkani, A. S.; Li, J.; Oliveira, N. J.; He, M.; Chang, X.; Xu, B.; Lu, Q. Understanding the Electric and Nonelectric Field Components of the Cation Effect on the Electrochemical CO Reduction Reaction. *Sci. Adv.* **2020**, *6*, eabd2569.